Solid Freeform Fabrication 2016: Proceedings of the 27th Annual International Solid Freeform Fabrication Symposium – An Additive Manufacturing Conference
Reviewed Paper

COMPLEX FUNCTIONAL SURFACE DESIGN FOR ADDITIVE MANUFACTURING

S. J. Morris[1], J. P. R. Dudman[1], L. Körner[1], P. Melo[1], L. H. Newton[1], A. T. Clare[2]

[1] Additive Manufacturing & 3D Printing Research Group, Uni. of Nottingham, NG7 2RD, U.K.
[2] Advanced Manufacturing Technology Research Group, Uni. of Nottingham, NG7 2RD, U.K.
e-mail: ezxsjm@nottingham.ac.uk (S. J. Morris)

ABSTRACT

This paper presents a new methodology for the creation of advanced surfaces which can be produced by Additive Manufacturing (AM) methods. Since there is no cost for enhanced complexity, AM allows for new capabilities in surface design. Micro-scale surface features with varying size, shape and pitch can be manufactured by Two-Photon Polymerisation (2PP). Computer-Aided Design (CAD) tools allowing for this variation to be incorporated into the surface design are only just emerging. With the presented methodology, surfaces are created from a single feature design. Variation is applied to the surface features through algorithmic design tools, allowing for arrays of hundreds of unique features can be created by non-CAD experts. The translation of these algorithmic expressions from CAD to a physical surface is investigated. Using the proposed methodology, 2PP is used to create quasi stochastic surfaces for the purpose of enhancing the biointegration of medical implants against current state-of-the-art.

1. INTRODUCTION

Modification of surface topology enables products to exhibit enhanced functionality [1]. Nature has long been a source of inspiration for tackling engineering challenges [2]. In 2003, Geim et al. [3] produced samples of micro-fabricated polyimide hairs to mimic keratin hairs found on gecko feet. These exhibited enhanced tactile properties for adhesion. In more recent research, Wen et al. [4] replicated shark denticles to reduce drag force. A single denticle design was patterned onto a flexible surface, resulting in a 6.6% increase in swim speed compared to smooth surfaces. In both studies, the features were of only one design type. In other words a common unit cell of fixed X, Y, Z dimension was created and then arranged in a uniform array with fixed X, Y pitches. This is illustrated in Figure 1 (a). Actual structures in nature exhibit natural variations in these parameters: for example shark denticles show a considerable difference in shape and pitch across the animals' body as well as across species [4]. Incorporating such variation into a surface array, as depicted in Figure 1 (b), could potentially improve biomimicry and further increase part performance.

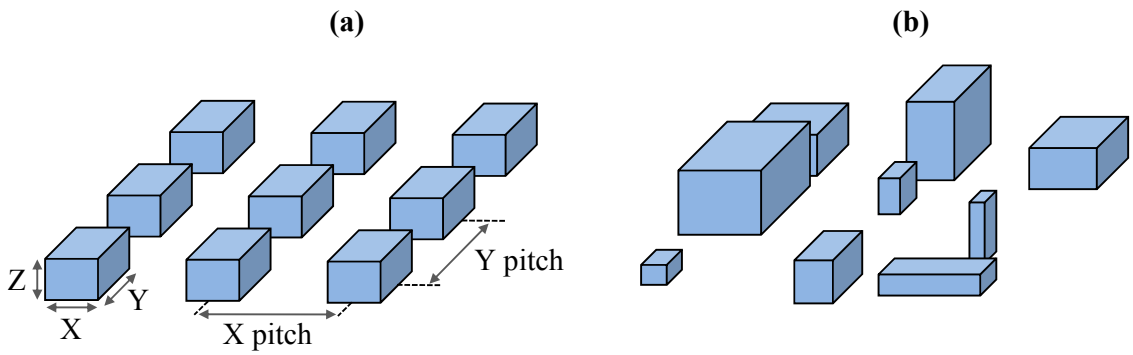

Figure 1: Diagrams illustrating parameters that define an array of surface features. (a) Surface features of the same X, Y, Z dimensions with the same X, Y pitches such as those created in [3-4]. (b) Surface features with varying X, Y, Z dimensions and X, Y pitches.

Regenerative medicine could significantly benefit from improved biomimetic surface design, allowing tissue scaffolds to better replicate the surrounding biological material when implanted. This could facilitate the regeneration of damaged or dysfunctional tissue. The interaction between cells and an implanted scaffold depends on surface topography amongst other factors, including surface chemistry. Studies determining cell response to simple features such as pits, grooves and pillars have yielded varying results, depending on: feature size, cell type and the manufacturing method used [5]. Some observed effects include increased cell adhesion, cell differentiation, directed growth and enhanced rates of spreading. Incorporation of nanoscale disorder into the spatial arrangement of surface features can lead to improved cell responses compared to ordered arrays such as: increased cellular adhesion and bone mineral production within mesenchymal stromal cell populations [6-7]. The ability to control the surface topology would allow for customised functionality of tissue scaffolds.

To build a surface with parametric variation requires a manufacturing technique that is able to produce these complex designs. Techniques such as transfer printing and laser ablation have been used to modify surfaces [8-9]. Whilst sub-100nm resolutions have been reported with transfer printing, the process requires the creation of a stamp for each new design. Both techniques are also limited in the possible structures that can be built due to being stamping and subtractive methods of processing. Additive Manufacturing (AM) does not require moulds or templates, building parts directly from CAD files [10]. Moreover AM grants greater geometric freedom, allowing for the creation of complex surface features unobtainable by traditional manufacturing techniques. This makes AM ideal for the production of surface features with a wide variation in morphology and spacing.

Current CAD tools are not tailored to designing surfaces with large numbers of non-identical surface features; simple patterning tools can replicate a feature and introduce variance from data defined in an external spreadsheet [11]. However this does not allow for synchronous design: where the CAD model is updated at the same time the user changes an input parameter. Currently users are required to know exactly what parameter values they desire beforehand, manually input these into the dataset, and wait for the model to update. Synchronous design,

gives the user visual feedback whilst designing, enabling a more intuitive and organic design process. Grasshopper® is an algorithmic modelling, visual programming plugin for Rhinoceros® CAD software. Parameters can be defined by mathematical expressions, allowing the geometric design of a large quantity of features to be changes simultaneously. The program allows for synchronous design and scripts with input controllers (such as sliders) to be written. This makes the design process more accessible to CAD novices.

In this paper, a methodology is proposed for designing complex surfaces that can be manufactured by AM. From a single surface feature design, arrays of said feature can be produced with variance in X, Y pitch and X, Y, Z dimensions. The variance can be normally distributed or defined by a mathematical expression. This allows for the creation of complex surfaces in a matter of minutes, whilst remaining user friendly. Arrays of one hundred pillars with varying diameters were fabricated by Two-Photon Polymerisation (2PP). The printed arrays were imaged with scanning electron microscopy and the diameters compared to the original CAD values to verify the ability of 2PP to accurately reproduce the designed variance. A case study is presented wherein surfaces are designed to increase biointegration of scaffolds for tissue engineering. Arrays of pillars and craters were produced by 2PP onto an existing part to determine the feasibility of 2PP as a method to improve existing scaffold surfaces.

2. EXPERIMENTAL METHODOLOGY

2.1 Two-Photon Polymerisation

2PP was chosen as the AM method to produce the designed surfaces as it is able to accurately build at the micron scale. A Nanoscribe™ Photonic Professional GT system was operated in Dip-In Laser Lithography (DILL) mode, a schematic of which is shown in Figure 2. The refractive index difference between the slide and photoresist is used to detect the slide surface and the build datum is set at this interface. To be found manually, practise builds were conducted at different build heights until the surface was found. Two-photon polymerisation occurs in the focal volume, the voxel, polymerising the photoresist. The piezoelectric scanning stage moves the slide relative to the fixed voxel.

The surfaces were built from the photoresist OrmoComp®, an organic-inorganic hybrid polymer shown in other studies to be biocompatible [12]. A mean laser power of 30mW was used for structures outer shells, 20mW for internal hatching with a scan speed of 20mm/s. The OrmoComp® was post-cured by heat treatment at 140°C for 10 minutes. OrmoDev® followed by an application of 2-isopropranol was used to remove excess material.

2.2 Verification Tests

Test arrays were designed and built to determine if 2PP could accurately reproduce the design intent at the required scales. Three arrays of one hundred pillars were designed, with each pillar given a X domain value between 0.01 and 1. The diameter of the pillars in microns (D) was then determined by the functions listed in Table 1. The exponential functions were

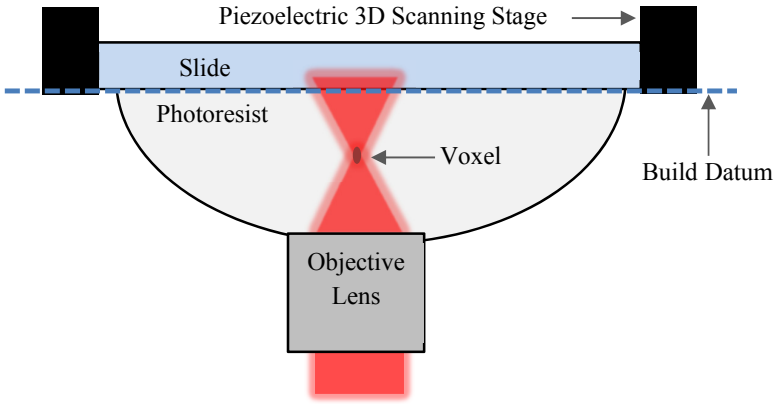

Figure 2: Schematic of the Dip-in Laser Lithography (DILL) mode used during two-photon polymerisation.

chosen to be of the same form ($D = Ae^{BX} + C$) to determine if the 2PP process can accurately reproduce the coefficient values A, B and C for each individual array. The arrays were built by 2PP in the method described in section 2.1 onto a glass slide. Scanning Electron Microscopy (SEM) was used to image the prints and from these ImageJ was used to determine the pillar diameters. The pillar diameters of the CAD design were then compared to those of the actual build.

	VT (1)	VT (2)	VT (3)
Function	$D = 2e^{2X}$	$D = 2e^{3X}$	$D = 2e^{2X} + 10$

Table 1: Functions used to define the pillar diameters (D) for the three verification test arrays.

2.3 Surface Modification for Tissue Scaffolds

2PP is limited by relatively slow build speeds. As such it may be more feasible for a tissue scaffold to be built by a quicker manufacturing method and the surface topography added in a second step by 2PP. This possibility was investigated by building arrays onto an existing part. 5x5mm Tri(Propylene Glycol) Diacrylate substrates, ~150µm in height, were used to simulate an existing tissue scaffold surface. The substrates were inkjetted by a PIXDRO™ Toucan and the designed arrays were then printed onto the substrate surface by 2PP using the method described in section 2.1. Existing topographies that have been found to enhance osteointegration – pillars and craters – were used as the surface features [5]. Three arrays were designed, applying normal distributions to the X Y pitches, height and diameters of the features. Images of the CAD designs are shown in Figure 3. Each array was built multiple times, allowing for large areas of the substrate surface to be modified. SEM was used to image the prints and qualitatively evaluate the builds.

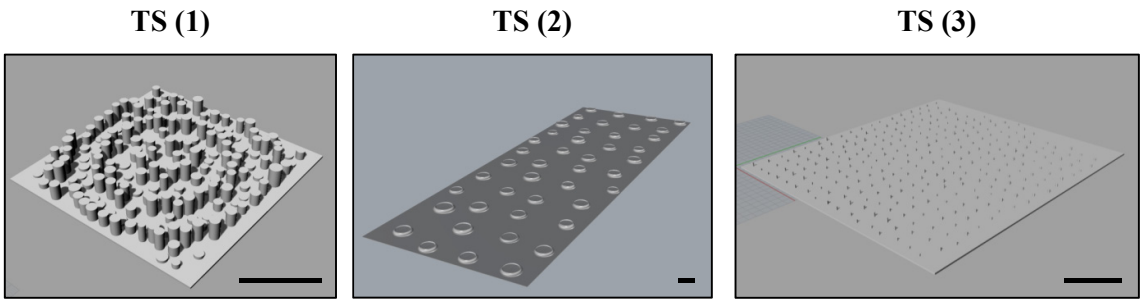

Figure 3: Designs of surface arrays to enhance biointegration of scaffolds. Features had their X Y pitches, diameter and heights normally distributed. The arrays were repeated in order to tile a large area of the substrate. TS (1): Pillar array on 112µm^2 base. A sinusoidal pattern was superimposed to produce the concentric ringed pattern seen. TS (2): Crater array on 500x1137µm base. Mean X Y pitches are 128±14µm, diameter 54±5µm and height 9±1µm. TS (3): Pillar array on 175x195µm base. Mean X Y pitches are 10.0±0.2µm, diameter 1.00±0.05µm and height 2.0±0.2µm. Scale bars = 50µm.

3. METHODOLOGY FOR SURFACE DESIGN

The developed methodology was based on the premise that it be able to apply and control variance to the surface features whilst being accessible for novice CAD users and not dramatically increasing design time. Grasshopper® was used to write the script for the surface design tool as it enabled synchronous modelling and the development of a basic Graphical User Interface (GUI). This allowed the stated objectives to be realised. In the script, the user can define the following parameters: X pitch, Y pitch and X Y Z bounding dimensions. These parameters can be varied for each surface feature either by a mathematical expression or by a normal distribution. The method for creating this quasi-normal distribution is visually demonstrated in Figure 4 .

The user defines the mean (μ), and standard deviation (σ) for the chosen parameter, labelled x in this example. The script then generates $\mathrm{N}/2$ values for a standard normal distribution z, where N is the total number of surface features in the array. The z values are shifted to x values by the following equation:

$$x = \mu + z\sigma \tag{1}$$

The values of z are generated in the following manner. Firstly n_i, the number of z values within the interval $z_i \rightarrow z_{i+1}$, is determined by the following equation:

$$n_i = \mathrm{round}\left(\frac{N}{2}\left[\int_0^{z_{i+1}} \mathrm{F}(z) - \int_0^{z_i} \mathrm{F}(z)\right]\right), \quad \{i \in \mathbb{Z}^+ | i > 0\} \tag{2}$$

where $\mathrm{F}(z)$ is the probability density of the standard normal distribution. The following intervals were used: 0 to 2 in steps of 0.1 and 2 to 6 in steps of 1, giving 24 intervals in total.

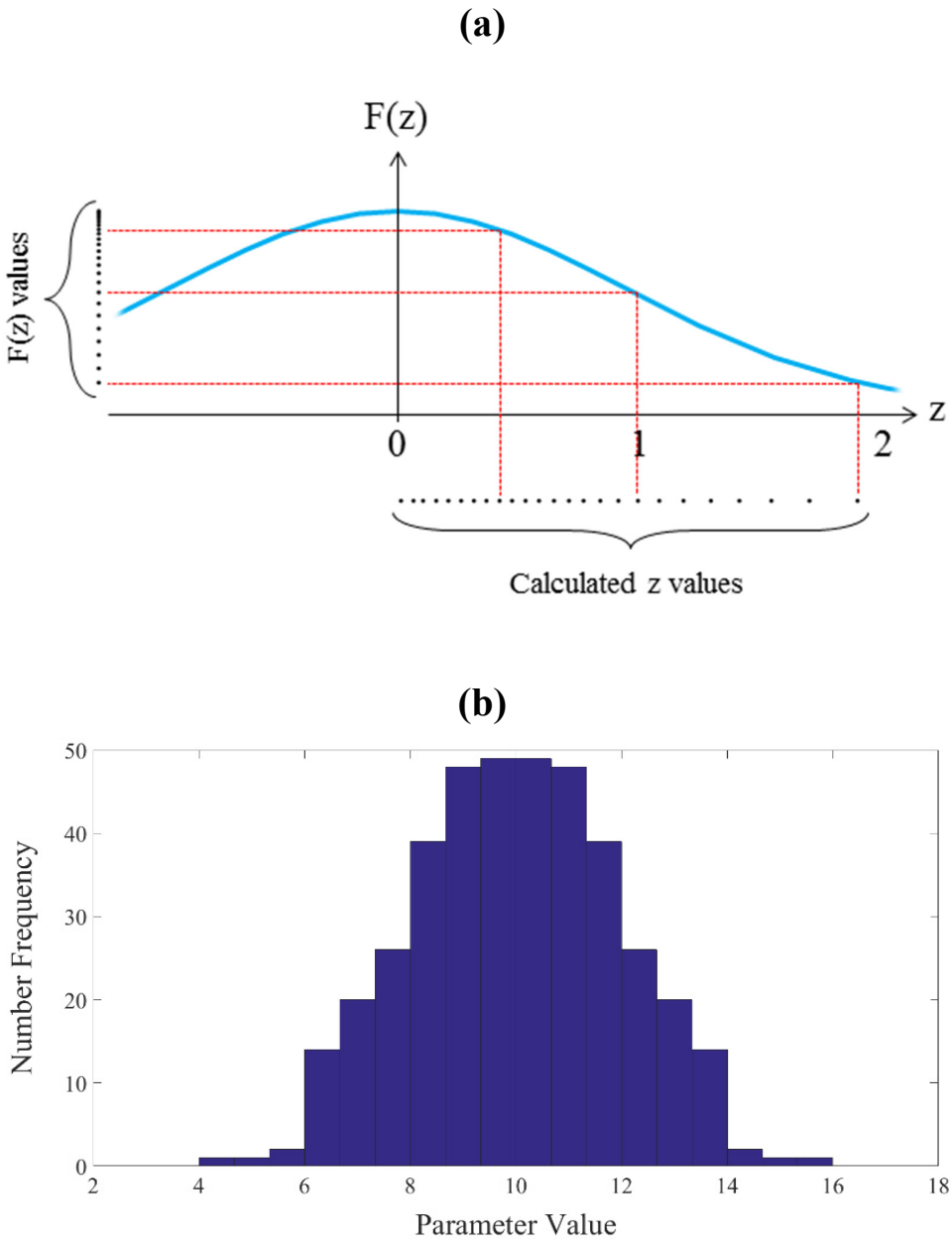

Figure 4: Diagrams illustrating how the script generates a quasi-normal distribution. (a) Equation (2) is used to determine the number of values within a given interval. Values of $F(z)$ are linearly spaced in these intervals, seen pictorially as the vertical set of points. From these, values of z (horizontal set of points) are calculated by equation (3). Intervals are represented by the dashed lines. (b) A histogram of four hundred parameter values. The user defined mean is 10, and standard deviation is 2. The actual mean of the generated distribution is 10.00 and 1.97 respectively, to two decimal places.

As this is the standard normal distribution the values of the integrals can be obtained from literature [13]. A simple normal distribution is used here but skew could be simply applied by manipulation of this function. The script then creates n_i equally spaced values of $\mathrm{F}(z)$ in each interval, as depicted by the vertical set of points in Figure 4 (a). From these the values of z are calculated by:

$$z = +\sqrt{-2\ln(\mathrm{F}(z)\sqrt{2\pi})} \tag{3}$$

This creates the $\mathrm{N}/2$ values of z, shown by the horizontal set of points in Figure 4 (a). These values are then shifted to the x parameter values by equation (1) and then reflected about the mean, giving the N normally distributed parameters values as shown in Figure 4 (b). As the generated distribution is discrete, not continuous, there will be a discrepancy between the generated standard deviation and that defined by the user. By linearly spacing values of $\mathrm{F}(\mathrm{z})$, values of z are not linearly spaced within the equivalent interval, as seen in Figure 4 (a). At larger values of N, this results in the generated standard deviation more closely matching the users' inputted value.

The steps of the proposed methodology are shown in Figure 5. The user starts with an unmodified surface, assumed to be a flat horizontal plane. A surface feature, such as the crater shown in Figure 5 (i), is designed through any CAD package before being imported into the script as an STL file. Using slider inputs, the user can define the number of surface features in X and Y directions. The X and Y pitches can be defined and given variance, by either mathematical expression or a normal distribution. The resultant array of coordinates, seen in Figure 5 (ii), act as centre point for each surface feature. The X, Y and Z bounding dimensions of the features can be distributed in the same manner. The result is an array of surface features with defined variation, an example of which is shown in Figure 5 (iii).

Then, if desired, an attractor point can be used to apply a user defined density increase to the array. An attractor point is placed on the array and a function is chosen using Grasshopper's interactive 'graph mapper' input. The distance between the attractor and array coordinates are scaled between 0.01 and 1, with 0.01 being the closet coordinate to the attractor. The function is then applied to whichever parameter the user desires. An example of such a pattern is shown in Figure 5 (iv). The script determines the new distribution of the altered parameter values, allowing the user to clearly see the final distribution.

Whilst not conducted here, this array could be applied to a conformal surface. This would allow for the surface to be incorporated onto an existing CAD part. The modified 'part' is then finalised and can be exported as an STL to be manufactured by a chosen AM method. This script allows for the modification of surfaces by creating arrays with hundreds of uniquely sized and spaced surface features in a matter of minutes.

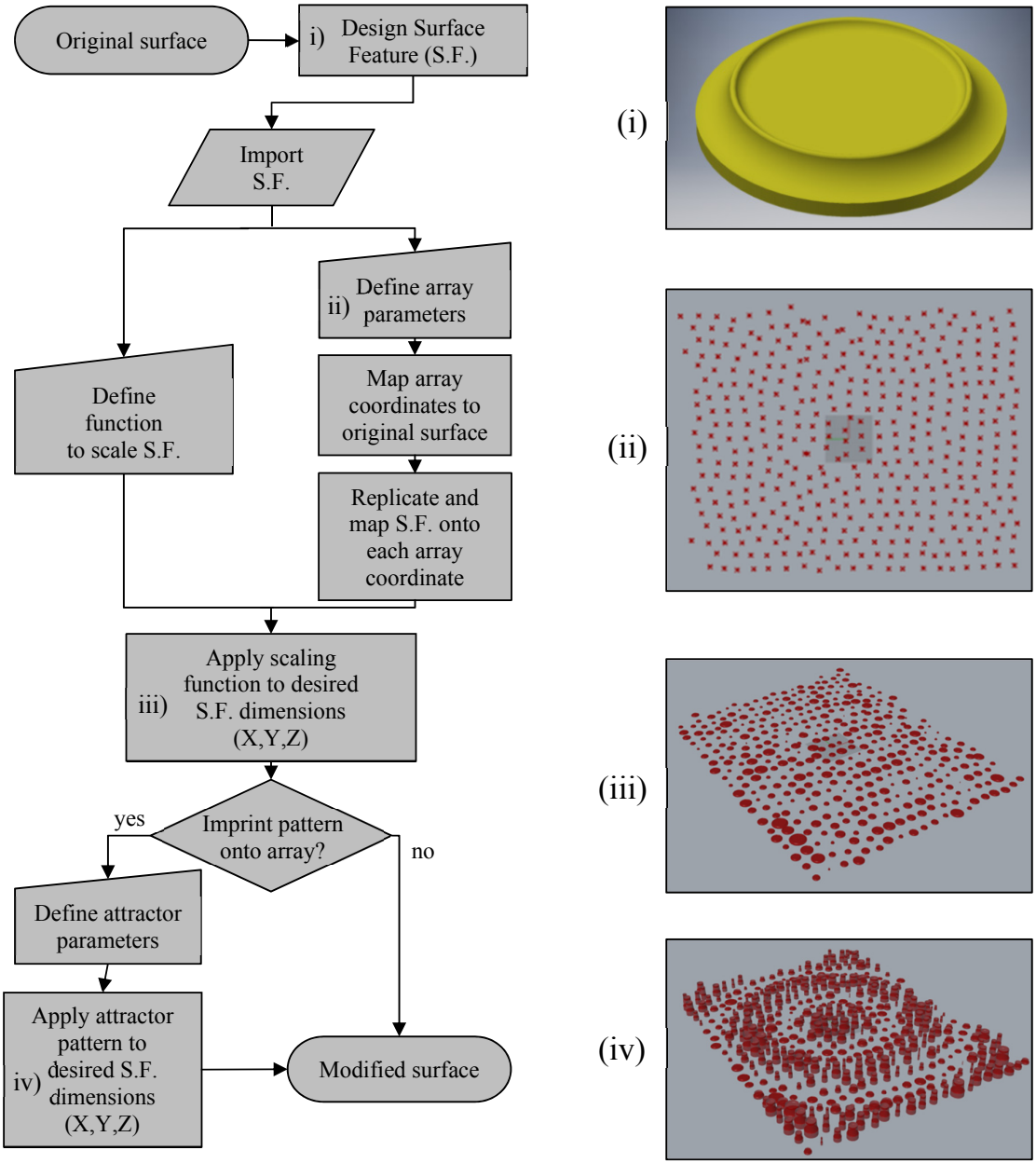

Figure 5: Flow Diagram of the proposed methodology to design complex surfaces. (i) Single surface feature design is imported into tool. (ii) Example of an array of coordinates that have had the X and Y pitches normally distributed. (iii) Example array of 400 craters with varying size and spacing. (iv) Example of a patterned array of 400 craters. The pattern was generated with an attractor point placed in the centre and sinusoidal function applied radially.

4. RESULTS

4.1 Verification Arrays

Figure 6 shows the results of the verification tests. The printed arrays VT (1) (ii) and VT (3) (ii) have debris on some of the pillars. These pillars were not included in the analysis. As can be seen in the (iii) graphs, there is an offset between the CAD design and printed diameters. The print is always larger than the CAD design, though the fidelity is fairly uniform across length scales.

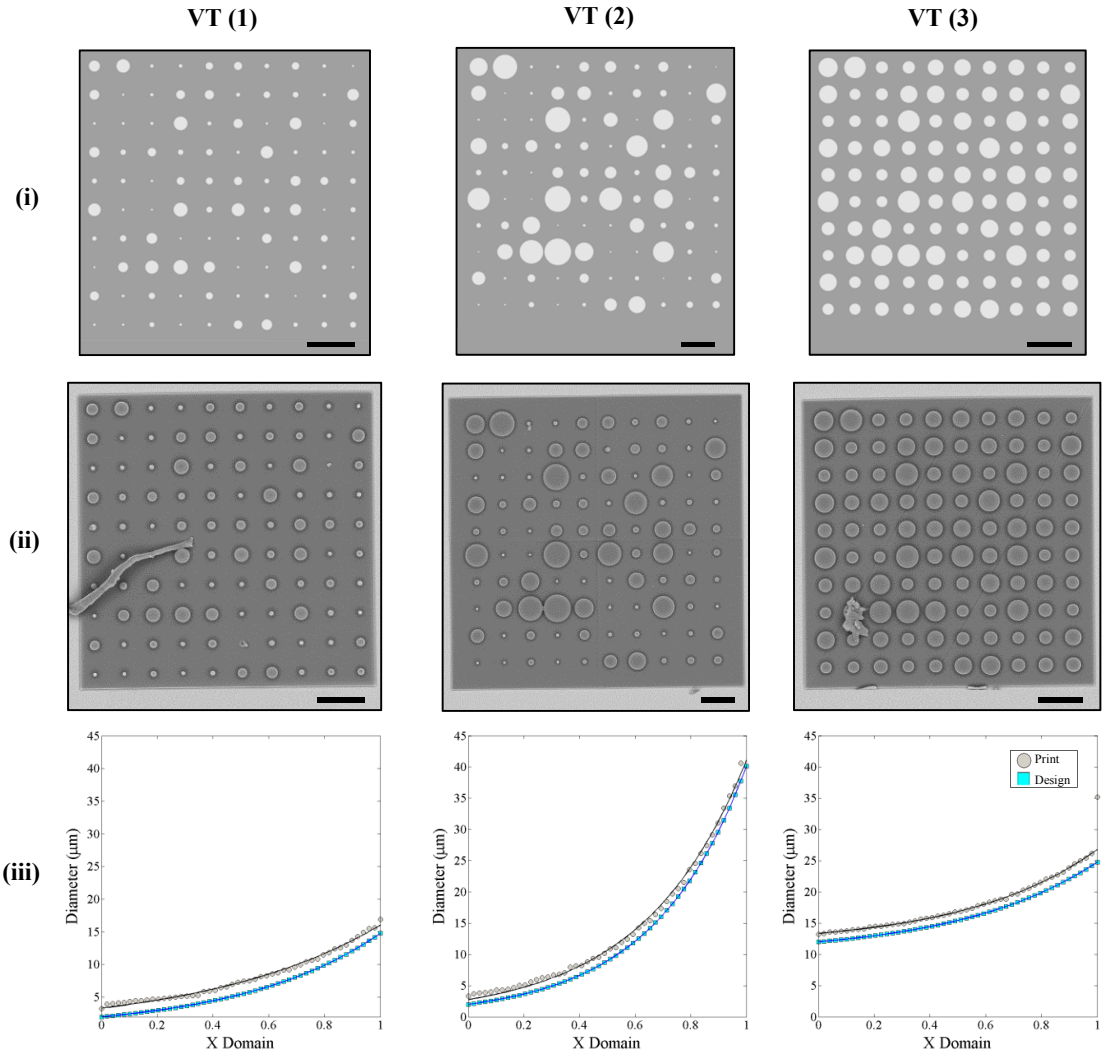

Figure 6: Comparison of design and printed test arrays. Each column corresponds to the labelled test array. (i) Top views of design arrays. (ii) S.E.M. images of 2PP printed arrays. (iii) Comparison of measured diameters on the print and design arrays. The print data was fitted with functions of the same input form and the coefficients presented in Table 2. Scale bars = 50µm.

For VT (1) (iii), the small pillars approach 0µm in diameter. The systems voxel size is ~200nm in x-y and ~1000nm in z, though this can be influenced by laser intensity, chosen focussing optics and photoresist material [14]. As such, diameters close the systems resolution limit cannot be accurately created. VT (2) (iii) shows as the diameter increases the offset between print and design is reduced. For VT (3) (iii) the offset appears consistent across all diameters, most likely due to the smallest diameters being much greater than the systems resolution. Whilst not quantitatively obtained, there will also be error introduced from the thresholding used during image analysis. This should be accounted for to more accurately determine any systematic error due to the Nanoscribe™ geometry interpretation algorithm.

Table *2* shows the fit parameters used for the CAD and printed arrays. The error on the print fit parameters range from ~0.5%-2.2%, indicating the 2PP process has precision systematic error which can therefore be compensated for. However, the discrepancy between the design fit parameters and print parameters is much larger for VT (1) and (2) than VT (3). This indicates building features close the systems resolution can have, as expected, a negative effect on the accuracy of the print designs.

	VT (1)		VT (2)		VT (3)		
Function	$D = ae^b$		$D = ae^b$		$D = ae^b + c$		
	a	b	a	b	a	b	c
Design	2	2	2	3	2	2	10
Print	3.32 ± 0.03	1.57 ± 0.01	2.76 ± 0.04	2.70 ± 0.02	1.86 ± 0.04	2.11 ± 0.02	11.50 ± 0.06

Table 2: Fit parameters for the design and print test arrays as seen in Figure 6. Error on print parameters from 1σ confidence bound of the computed fit.

4.2 Tissue Scaffold Surface Modifications

Figure 7 shows S.E.M images of the 2PP prints of the tissue scaffold surfaces. TS (1) print took ~7 minutes to build an area of 336µm^2. TS (1) (iii) shows the concentric rings produced by the attractor and the variation in pillar height produced. Comparing to the CAD design in Figure 3, the top of the printed pillars became rounded, due to the resolution of the system and the ellipsoidal shape of the 2PP voxel.

TS (2) build is 500µm x 1137µm and took ~15 minutes to build. TS (2) (i) shows the designs base appearing to fade into the substrate. This is due to printing onto a non-flat substrate surface with a flat, fixed height build datum. This is shown schematically in Figure 8. This can lead to build errors as seen in TS (2) (iii), where misalignments between build sections have caused the crater halves to not join.

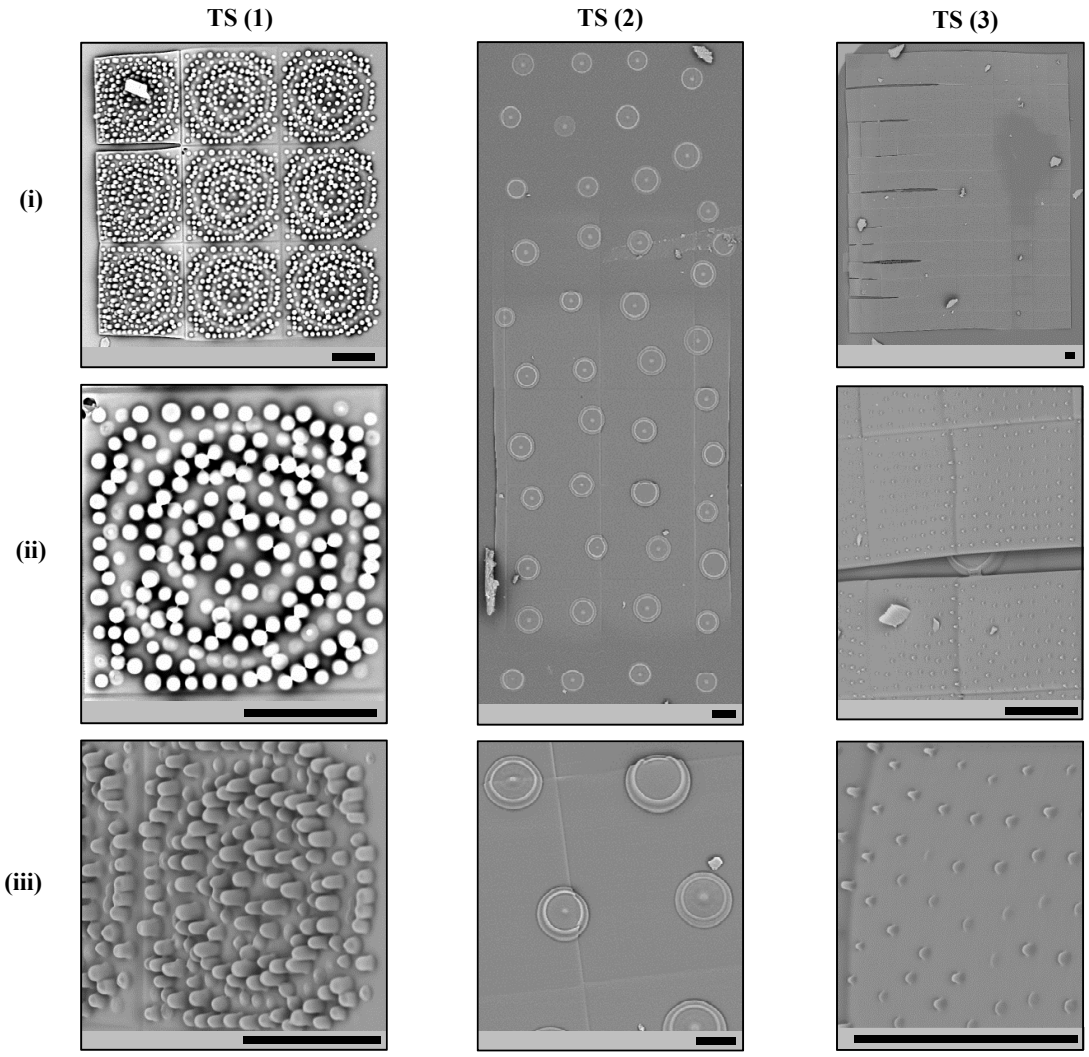

Figure 7: S.E.M images showing the printed surface arrays for enhanced biointegration. TS (1): (i) 3x3 grid of the repeated CAD design. (ii) Centre pattern. (iii) Side view of the centre right pattern. TS (2): (i) Top view of printed surface. The substrates surface can be seen to rise above the build datum where the base plate disappears. (iii) Error in the section alignment leads to parts of craters split over two build sections not joining up. TS (3): (i) 6x8 grid of the repeated CAD design. The design was split into four sections and as such consists of 12x16 squares with the design repeating every two squares. (ii) Section where substrate surface falls away from the build datum, leading to a split in the grid. (iii) Side view of pillars. Scale bars = 50µm.

TS (3) took ~45 minutes to build the 1400µm x 1170µm design. As seen in TS (3) (i) sections have not joined properly on the left side of the array. At the edge of the substrate, the substrates surface drops dramatically below the build datum, leaving the printed sections here to drift freely down to the surface. This results in the large misalignments seen. Additionally a faded patch can be seen to the right of the build, due to the substrates surface rising above the build datum. TS (3) (ii) shows how similar faults can arise from building on top of existing surface features. A closer view of the pillars is seen in TS 3 (iii).

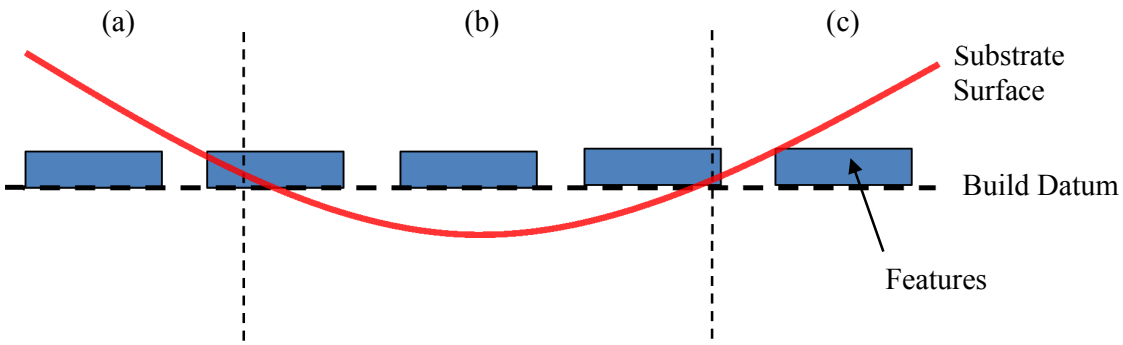

Figure 8: Schematic showing how building on a non-flat substrate surface can lead to build errors. In (a) and (c), the substrate surface has risen above the build datum leading to features being built below, not on, the substrate surface, resulting in 'faded patches' as seen in Figure 7 TS (2) (i) and TS (3) (i). In (b) the surface has fallen below the build datum. Features are built unattached above the surface before drifting freely down to the surface. This can cause misalignments and deformations in the build, as seen in Figure 7 TS (2) (iii) and TS (3) (i) & (ii).

Being close to the resolution of the system, the pillars have lost the defined 'pillar shape' of the CAD design. This is variation that is not designed for, and is a limitation of the manufacturing method. These results emphasise the importance of the existing surfaces texture has when attempting to modify a surface with 2PP.

5. DISCUSSION

The proposed methodology simplifies what could otherwise be a complex process by using algorithmic programming to set up a large array of varied surface features. Grasshopper® working synchronously with Rhinoceros® makes the design process intuitive and user friendly to non-CAD experts. This methodology for surface modification can be applied to challenges other than those presented in this project, for example improving parts fluid dynamics or fatigue performance. Moreover, the methodology can be adapted for areas other than surface design, allowing for variance and mathematical expression to be easily incorporated into CAD parts.

More work can be conducted in order to improve capabilities of the presented methodology. Collision detection between surface features can be incorporated to ensure overlaps do not occur, which could lead to build errors during manufacture. As seen in the tissue scaffolds case study, error in the build can arise due to a non-flat substrate surface. Producing mathematical models or direct surface measurements of the substrate would allow the array to be mapped onto the surface. In addition the surface features are only squashed or stretched in X, Y and Z. By building the surface feature within Grasshopper® itself, it would allow for parts of the surface features to be scaled independently, instilling more detailed and controlled variation in the surface features.

The verification tests and case study highlight the limitations and issues needed to be overcome using 2PP to manufacture complex surfaces. Surface features close to the resolution

of the system are reproduced less accurately. Avoiding features of size ~1μm will improve the accuracy and reproducibility of the build. The systematic error between design and print should be quantified and included in the design process to allow for the features to come out at the desired size.

Complications arose when attempting to modify the substrate surfaces; misalignment between build sections or missing features arose due to building on an undulating substrate surface with a single flat datum of fixed height. The Nanoscribe™ Photonic Professional GT has an interface finder capability, which did not work in this case study due to an insufficient difference in the refractive index of TPGDA and OrmoComp®. Appropriate choices of material could allow this function to be implemented, allowing each build sections datum to be located onto the substrates surface.

6. CONCLUSION

A methodology for conducting complex surface design has been presented. A script was written that used algorithmic programming to incorporate variation into a surface, allowing for arrays of hundreds of uniquely sized and spaced features to be created from a single surface feature design. This can be built by AM, allowing complex surfaces to be implemented without an unreasonable increase in design or lead time. The ability to create complex, functional surfaces has uses in many design areas, for example improving parts fluid flow or fatigue performance. This methodology enables novel surface designs to be feasibly created for these applications. Further work can be undertaken to add more capabilities to the script, such as the ability to scale parts of surface features independently, creating a more powerful design tool.

Verification tests demonstrate that 2PP is a viable process to precisely build the surface design at the microscale. Whilst close in accuracy to the original CAD sizes, this could be improved by quantifying any systematic error and then offsetting this within the actual CAD design. A case study for the surface modification of tissue scaffolds to enhance biointegration was conducted. Mesoscale arrays were printed onto an existing substrate, demonstrating the feasibility of such modification. Errors with array alignment due to a non-flat substrate surface need to be addressed to improve accuracy and reproducibility. With future developments, the presented methodology may enable healthcare professionals to selectively design custom scaffold surfaces prior to manufacturing, allowing for higher performing tissue scaffolds without huge rises in cost and lead time.

Whilst in the preliminary stages, the methodology demonstrates the freedom of design and complexity achievable with AM surfaces with the appropriate CAD tools. Such algorithmic methods can open up new design possibilities, having significant future applications for surface modification to improve part performance.

7. ACKNOWLEDGEMENTS

Thanks to the EPRSC (Engineering and Physical Sciences Research Council) Centre of Doctoral Training in Additive Manufacturing and 3D Printing for support and funding. Thanks to Dr Qin Hu and Benjamin Paul for their support with the Nanoscribe™ Photonic Professional GT and Dr Ehab Saleh for providing the substrates printed on the PIXDRO™ Toucan.

REFERENCES

[1] G. G. Fuentes, "Surface Engineering and Micro-manufacturing," in *Micromanufacturing Engineering and Technology*, 2nd ed., Y. Qin, Ed. William Andrew, 2015, pp. 459–486.

[2] Y. Bar-Cohen, "Nature as a Model for Mimicking and Inspiration of New Technologies," *Int. J. Aeronaut. Sp. Sci.*, vol. 13, no. 1, pp. 1–13, 2012.

[3] A. K. Geim, S. V. Dubonos, I. V. Grigorieva, K. S. Novoselov, A. A. Zhukov, and S. Y. Shapoval, "Microfabricated adhesive mimicking gecko foot-hair," *Nat. Mater.*, vol. 2, pp. 461 – 463, 2003.

[4] L. Wen, J. C. Weaver, and G. V. Lauder, "Biomimetic shark skin: design, fabrication and hydrodynamic function," *J. Exp. Biol.*, vol. 217, pp. 1656–1666, 2014.

[5] U. Meyer, T. Meyer, J. Handschel, and H. P. Wiesmann, Eds., *Fundamentals of Tissue Engineering and Regenerative Medicine*. Berlin: Springer, 2009.

[6] A. S. G. Curtis, N. Gadegaard, M. J. Dalby, M. O. Riehle, C. D. W. Wilkinson, and G. Aitchison, "Cells React to Nanoscale Order and Symmetry in Their Surroundings," *IEEE Trans. Nanobioscience*, vol. 3, no. 1, pp. 61–65, 2004.

[7] M. J. Dalby, N. Gadegaard, R. Tare, A. Andar, M. O. Riehle, P. Herzyk, C. D. W. Wilkinson, and R. O. C. Oreffo, "The control of human mesenchymal cell differentiation using nanoscale symmetry and disorder," *Nat. Mater.*, vol. 6, no. 12, pp. 997–1003, 2007.

[8] D. Bhandari, I. I. Kravchenko, N. V Lavrik, and M. J. Sepaniak, "Nanotransfer Printing Using Plasma Etched Silicon Stamps and Mediated by in Situ Deposited Fluoropolymer," *J. Am. Chem. Soc.*, vol. 133, no. 20, pp. 7722–7724, 2011.

[9] M. Malinauskas, S. Rekštyt˙ E, L. Lukoševičius, S. Butkus, E. Balči, ¯. Unas, M. Pečiukaityt˙ E, D. Baltriukien˙ E, V. Bukelskien˙ E, A. ¯. Unas Butkevičius, P. Kucevičius, V. Rutk, and S. Juodkazis, "3D Microporous Scaffolds Manufactured via Combination of Fused Filament Fabrication and Direct Laser Writing Ablation," *Micromachines*, vol. 5, pp. 839–858, 2014.

[10] M. Baumers, P. Dickens, C. Tuck, and R. Hague, "The cost of additive manufacturing: Machine productivity, economies of scale and technology-push," *Technol. Forecast. Soc. Change*, vol. 102, pp. 193–201, 2016.

[11] NX Tutorials, "NX8 Pattern with Spreadsheet," 2011. [Online]. Available: nxtutorials.com/2011/09/nx8-pattern-with-spreadsheet/. [Accessed: 10-Jun-2016].

[12] S. Schlie, A. Ngezahayo, A. Ovsianikov, T. Fabian, H.-A. Kolb, H. Haferkamp, and B. N. Chichkov, "Three-Dimensional Cell Growth on Structures Fabricated from ORMOCER(R) by Two-Photon Polymerization Technique," *J. Biomater. Appl.*, vol. 22, no. 3, pp. 275–287, 2007.

[13] J. E. Freund, *Mathematical Statistics*, 5th ed. Prentice Hall, 1992.

[14] M. Thiel and M. Hermatschweiler, "Three-dimensional laser lithography," *Opt. Photonik*, vol. 6, no. 4, pp. 36–39, 2011.